Astronomy & Astrophysics manuscript no. sp11
January 8, 2010

© ESO 2010

arXiv:0911.3319v3 [astro-ph.SR] 8 Jan 2010

On the power spectrum of solar surface flows

M. Rieutord[1], T. Roudier[1], F. Rincon[1], J.-M. Malherbe[2], N. Meunier[3], T. Berger[4] and Z. Frank[4]

[1] Laboratoire d'Astrophysique de Toulouse-Tarbes, Université de Toulouse, CNRS, 14 avenue E. Belin, 31400 Toulouse, France
[2] LESIA, Observatoire de Paris, Section de Meudon, 92195 Meudon, France
[3] LAOG, Université Joseph Fourier, CNRS, BP 43, 38041 Grenoble Cedex, France
[4] Lockheed Martin Advance Technology Center, Palo Alto, CA, USA
e-mail: `[rieutord,roudier,rincon]@ast.obs-mip.fr`, `Jean-Marie.Malherbe@obspm.fr`, `nmeunier@obs.ujf-grenoble.fr`, `berger@lmsal.com`, `zoe@lmsal.com`

January 8, 2010

ABSTRACT

Context. The surface of the Sun provides us with a unique and very detailed view of turbulent stellar convection. Studying its dynamics can therefore help us make significant progress in stellar convection modelling. Many features of solar surface turbulence like the supergranulation are still poorly understood.
Aims. The aim of this work is to give new observational constraints on these flows by determining the horizontal scale dependence of the velocity and intensity fields, as represented by their power spectra, and to offer some theoretical guidelines to interpret these spectra.
Methods. We use long time-series of images taken by the Solar Optical Telescope (SOT) on board the Hinode satellite; we reconstruct both horizontal (by granule tracking) and vertical (by Doppler effect) velocity fields in a field-of-view of $\sim 75{\times}75$ Mm^2. The dynamics in the subgranulation range can be investigated with unprecedented precision thanks to the absence of seeing effects and the use of the modulation transfer function of SOT for correcting the spectra.
Results. At small subgranulation scales down to 0.4 Mm the spectral density of kinetic energy associated with vertical motions exhibits a $k^{-10/3}$-like power law, while the intensity fluctuation spectrum follows either a $k^{-17/3}$ or a k^{-3}-like power law at the two continuum levels investigated (525 and 450 nm respectively). We discuss the possible physical origin of these scalings and interpret the combined presence of $k^{-17/3}$ and $k^{-10/3}$ power laws for the intensity and vertical velocity as a signature of buoyancy-driven turbulent dynamics in a strongly thermally diffusive regime. In the mesogranulation range and up to a scale of 25 Mm, we find that the amplitude of the vertical velocity field decreases like $\lambda^{-3/2}$ with the horizontal scale λ. This behaviour corresponds to a k^2 spectral power law. Still in the 2.5–10 Mm mesoscale range, we find that intensity fluctuations in the blue continuum also follow a k^2 power law. In passing we show that granule tracking cannot sample scales below 2.5 Mm. We finally further confirm the presence of a significant supergranulation energy peak at 30 Mm in the horizontal velocity power spectrum and show that the emergence of a pore erases this spectral peak. We tentatively estimate the scale height of the vertical velocity field in the supergranulation range and find 1 Mm; this value suggests that supergranulation flows are shallow.

Key words. Convection – Turbulence – Sun: photosphere

1. Introduction

A complete understanding of thermal convection in stars remains one of the main challenges of present day astrophysics. The Sun offers an unsurpassed detailed view to address this question. Solar convection is highly non-linear – typical Reynolds numbers are over 10^{10} – making fully detailed direct numerical simulations down to the viscous dissipation scales unaffordable. In spite of this difficulty, some observed features of solar convection like for instance granulation are rather well understood (e.g. Stein & Nordlund 2000). Dynamical features at larger scales like the supergranulation pattern are much less understood. Supergranulation is characterised by a horizontal velocity field spanning scales from 15 Mm to 75 Mm according to the recent work of Rieutord et al. (2008). Despite several attempts, supergranulation has not been identified in large-eddy or direct numerical simulations (e.g. Rieutord et al. 2002; Rincon et al. 2005; Stein et al. 2009). Its origin remains unknown, although some scenarios have been proposed. The classical picture (Simon & Leighton 1964) is a linear thermal convection scenario which associates supergranulation cells with the second ionisation of helium. Other scenarios put forward the idea that supergranulation is a surface phenomenon, as actually indicated by the recent results of local helioseismology (Gizon & Birch 2005). Rieutord et al. (2000) suggested that it could be the result of a large-scale instability of surface granular convection. Rincon & Rieutord (2003) proposed that some fixed flux boundary condition is imposed by the granulation to the layers just below: with these boundary conditions, the buoyancy destabilises the largest available scales. The associated convective motions have a fairly low intensity contrast (van der Borght 1974), very much like supergranulation cells (Meunier et al. 2007). Rincon & Rieutord (2003) further showed that an effective finite but large horizontal convection scale can be obtained in this framework by considering the dynamical effects of a mean magnetic field on the flow. Collective plume interactions (Rast 2003; Crouch et al. 2007) and travelling-wave sheared (Green & Kosovichev 2006) convection or magnetoconvection (Green & Kosovichev 2007) have also been suggested as a possible origin of supergranulation.

Send offprint requests to: M. Rieutord

Overall the constraints on the large-scale dynamics of solar convection imposed by models and theories are still very loose. Guidance from observations is thus much desired. Particularly if a dynamical connection exists between granulation and supergranulation, some hints of such a scale interaction should be found in the dynamics of intermediate horizontal scales. Flows in the 3–10 Mm range are little known. This range of scales is traditionally referred to as the mesogranulation range after the work of November et al. (1981), but the very existence of genuine enhanced convective motions at these scales has been much debated (Straus et al. 1992; Straus & Bonaccini 1997; Rieutord et al. 2000; Shine et al. 2000). As pointed out in Rieutord et al. (2000), the main problem with mesogranulation was its way of detection, namely through the measurement of the horizontal divergence of the flows, which is highly sensitive to the way data are reduced. The very nature of the flows at these scales is nonetheless important to answer the question of the origin of supergranulation.

In order to make progress, it is clear that the large-scale side of the granulation spectral peak should be investigated in more detail. Simple models like the mixing-length theory or plume dynamics (Rieutord & Zahn 1997) do not predict any special spectral feature when the scale (horizontal or vertical) grows. Hydrodynamic numerical simulations like the recent ones of Stein et al. (2009) seem to go in the same direction and do not exhibit any spectral feature reminiscent of supergranulation (see also Nordlund et al. 2009). However, kinetic energy spectra derived from the radial velocity measured by SOHO/MDI (i.e. from dopplergrams) do show a rise of the spectral kinetic energy density at a scale of 11 Mm and a peak at 36 Mm (Hathaway et al. 2000). These results are clearly confirmed by the recent measurement of the horizontal surface flows at disc centre with the wide-field high resolution camera CALAS at Pic-du-Midi (Rieutord et al. 2008). These observations are therefore clearly at odds with the most advanced numerical models of solar surface convection.

In this paper we wish to provide accurate observational facts to guide modelling efforts and impose more constraints for theories. For this purpose we use new data sets collected by the Hinode mission and especially by the SOT instrument. Because of their high spatial resolution and their very low noise, these data are appropriate to either refine previous measurements or investigate new properties of the flows. In particular the subgranulation range can now be investigated as never before. We shall focus our attention on the power spectra of the flows because the information that can be obtained from such representations is usually the most robust aspect of these highly turbulent flows.

The paper is organised as follows: after a brief presentation of the data and the techniques to process them (Sect. 2), we detail the spectral properties of the measured velocity fields (Sect. 3) and the intensity field (Sect. 4). A discussion and physical interpretation of the results follows (Sect. 5). The main results and conclusions are summarised at the end of the paper (Sect. 6).

2. The data and the reduction procedure

We used multi-wavelength data sets of the Solar Optical Telescope (SOT) on board the HINODE[1] mission (e.g. Ichimoto et al. 2004; Suematsu et al. 2008). The SOT has a 50 cm primary mirror with a spatial resolution about 0.2″at 550 nm.

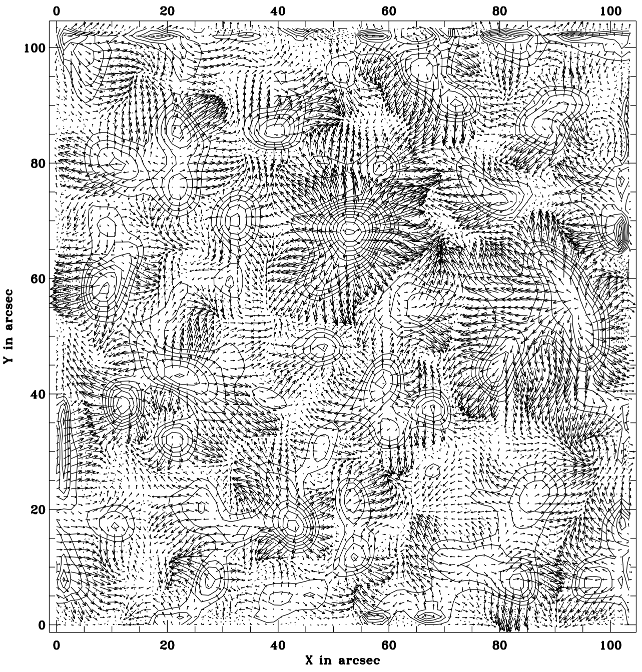

Fig. 1. Velocity field derived from the motion of granules during a 45 min window, interpolated by a Daubechies wavelet of 4*953 km. Contours mark the horizontal divergence of the velocity.

2.1. Horizontal velocities

A first set of images taken at disc centre was recorded continuously from 29 August 10:17 UT until 31 August 10:19 UT 2007, except for an interruption of seven minutes on 30 August at 10:43 UT. We used the set taken with the broad-band filter imager (BFI) with a spectral width of 0.22 nm (Wedemeyer-Böhm & Rouppe van der Voort 2009) in the blue continuum at 450.45 nm. The mean time step between two successive frames is 50.1 sec. The field-of-view with BFI is 111.″6 × 111.″6 with a pixel of 0.″109 (1024 × 1024). After alignment, the useful field-of-view was reduced to 104.″6 × 104.″6 or 76.3 × 76.3 Mm^2 during 33h. The data were also $k-\omega$ filtered with a phase velocity threshold of 6 km s^{-1} to keep only convective motions.

We determined the horizontal velocity field for various time averages from this set of data, using our algorithm of granule tracking CST (Rieutord et al. 2007). We recall that because of the nature of granules their motion is representative of the large-scale plasma flow only for length scales larger than 2.5 Mm and time scales longer than 30 min. These limits have been derived from numerical simulations by Rieutord et al. (2001) and are confirmed by these data (see below).

Other data sets were processed in the same way to compare several flow characteristics (see Table 1).

2.2. Vertical velocities

To determine the vertical component of the velocity we used a second data set from SOT/Hinode, also taken at disc centre and recorded on 4 September 2009 21:08 UT to 22:25 UT. These

---

[1] The Hinode spacecraft launched in 2006 was designed and is now operated by JAXA (Japanese Space Authorities) in cooperation with NASA (National Aeronautics and Space Administration) and ESA (European Space Agency).

Table 1. The position and amplitude of the supergranulation peak for various data sets.

Date	Instrument	FOV (Mm^2)	Filter	Time slot	λ_{SG} (Mm)	E_{SG} (km^3/s^2)
			Wide-field data			
1996 May-Jul	SOHO/MDI	global	Ni I, 676.8 nm	62d	36.4	(200)
2000 Apr 22	TRACE	225x250	WL	6x3 h	35.6	200
2007 Apr 24	TRACE	238x275	WL	2x3.4 h	29.8	490
2007 Mar 13	CALAS	290x216	575 nm	2x3 h	36.4	350
			Small-field data			
2007 Mar 8	Hinode/SOT	75.9x76.8	G-band	4h	no peak	220
2007 Mar 15	Hinode/SOT	77.3x33.9	G-band	3x3h	57/17-27	240/350
2007 Aug 29-30	Hinode/SOT	76.6x76.6	blue	11x3h	28.7	600
2007 Oct 1	Hinode/SOT	2x(76x76)	blue	2x3.8h	27/31	460/545

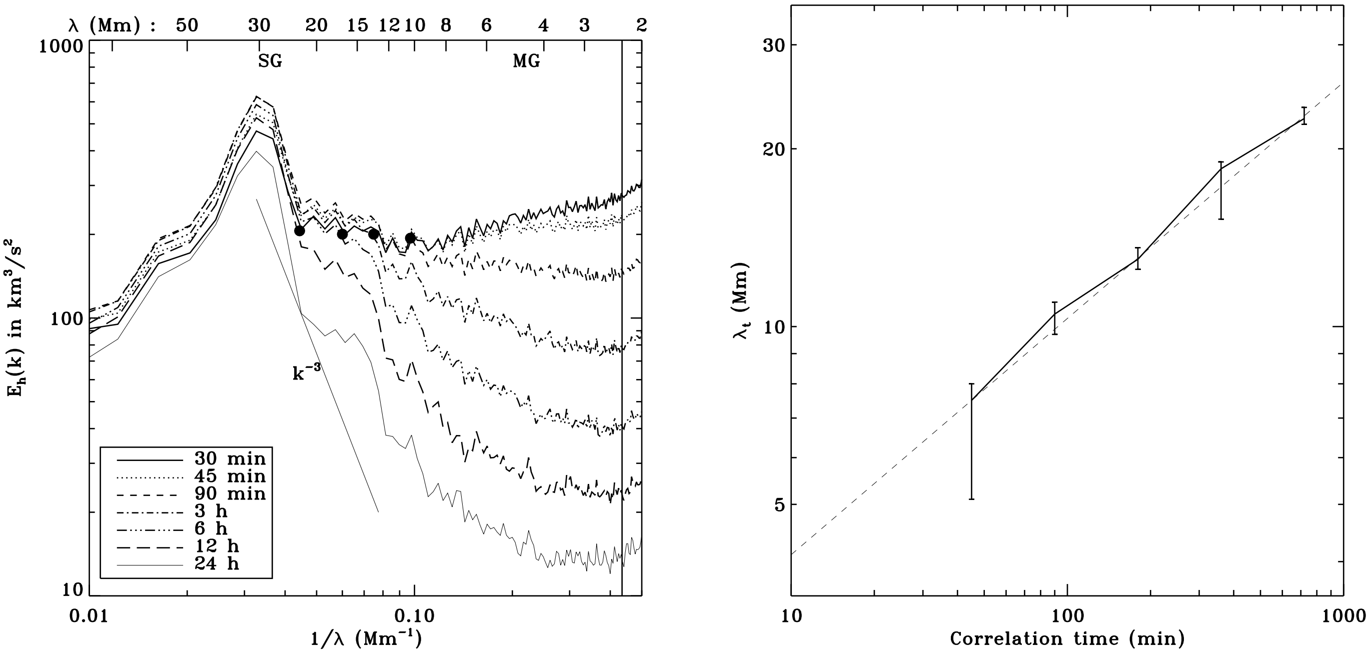

Fig. 3. Left: kinetic energy spectra of the horizontal velocity field for various time windows. The vertical line marks the 2.3 Mm scale below which noise dominates. The black dots mark the scale at which the spectrum of a given time average disconnects from the 30-min one. Right: relationship between the length scale and the correlation time scale for the horizontal velocity field. Here $N_x = N_y = 80$ and $N_p = 256$.

data were taken with the narrowband filter imager (NFI) with a spectral width of 9 pm, near the FeI line at λ_0 =557.6 nm, sampling nine wavelengths in the line profile. This regular sampling allowed us to accurately measure the Doppler shift of the line every 28.5s. The field-of-view of this series is $82'' \times 82''$, which represents 60×60 Mm^2. The pixel size is $0\farcs08$.

These data are completed by a third data set from SOT/Hinode, taken at disc centre and recorded on 4 September 2009 7:35 UT to 10:17 UT with a regular cadence of one image every 57.5 s. These data were also obtained with the NFI but around the FeI line at 525.0208 nm. However, in that case the line profile was sampled only at two wavelengths, namely $\lambda_0 - 1.8$ pm and $\lambda_0 + 10.8$ pm, which did not allow us to determine the Doppler shift of the line in the same way as with the second data set. The radial velocity was instead estimated through the simple relationship

$$v = k\frac{I_b - I_r}{I_b + I_r} + v_0\,, \tag{1}$$

where v_0 and k are constants and I_r and I_b are the intensities in red and blue positions of the filter (+10.8 pm and −1.8 pm) respectively. The actual relationship between the radial velocity and the intensity difference for this particular line and positions of the filter is shown in Fig. 4. Note that an unavoidable pitfall with NFI is that the red and blue positions of the filter are in general asymmetric with respect to λ_0. From the previous plot we see that this implies that large velocities cannot be measured correctly on one side of the line for these data (here on the blue side). The field-of-view of this series is $112\farcs6 \times 112\farcs6$ with a pixel of $0\farcs16$, corresponding to a physical field of 82×82 Mm^2.

The Doppler fields were then $k - \omega$ filtered to remove fast horizontal motions of the patterns with a threshold of 6 km s^{-1}.

Unfortunately no flat-field image was available for the data sets taken at λ_0 =557.6 nm. We tried to circumvent this problem by creating a flat-field image for each image. For this purpose we averaged 50 images around the desired one and smoothed the result with a window of $16''\times16''$. The operation possibly altered the signal at scales larger than 12 Mm. Note finally that unlike the λ_0 =557.6 nm data sets, we were able to correct the

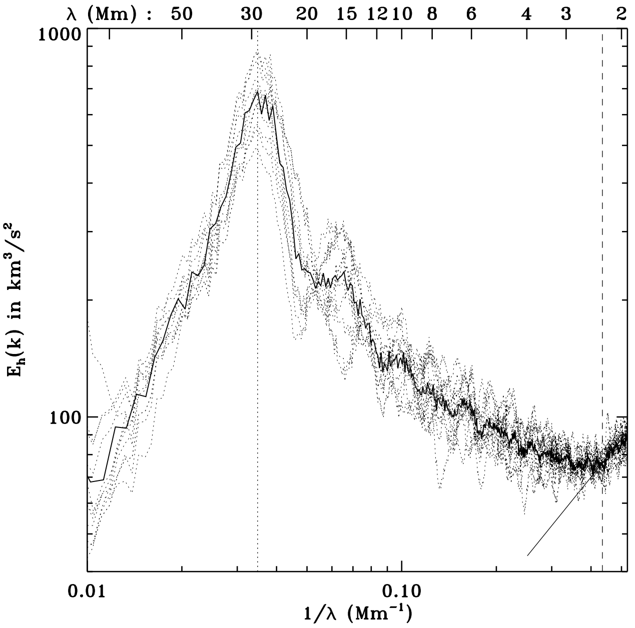

Fig. 2. Mean spectra and fluctuations: eleven independent horizontal kinetic energy spectra (dotted lines) computed with a three-hours time window, along with their average (thick solid line) are represented. Note that the fluctuations may reach an amplitude of 40% compared to the mean value. The straight line on the right indicates the power law $E(k) \sim k$ characteristic of decorrelated noise. The vertical straight line marks the 2.3 Mm scale. Here $N_x = N_y = 80$ and $N_p = 1024$.

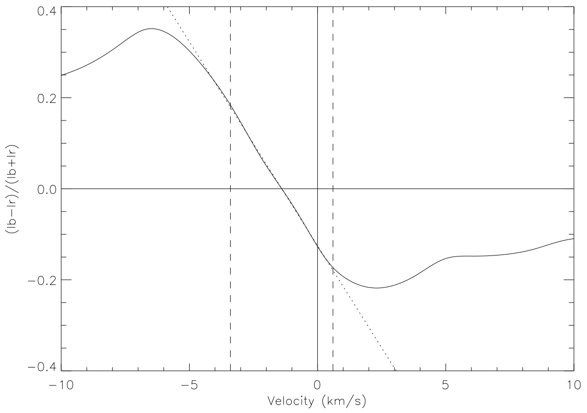

Fig. 4. Relationship between radial velocities and relative intensity fluctuations, using the two wavelengths at -1.8 pm and +10.8 pm aside the FeI line at 525 nm. Positive velocities are towards the observer.

data set taken around λ_0 =525.0 nm with a genuine flat-field image.

Finally, following Danilovic et al. (2008) we computed the PSF and MTF of SOT to deconvolve all the images including those used to derive the Doppler shift from the instrument effects (central obscuration, spider and ccd). This correction turned out to be crucial for the investigation of subgranulation-scale turbulence, which is one of the novelties brought by the Hinode mission.

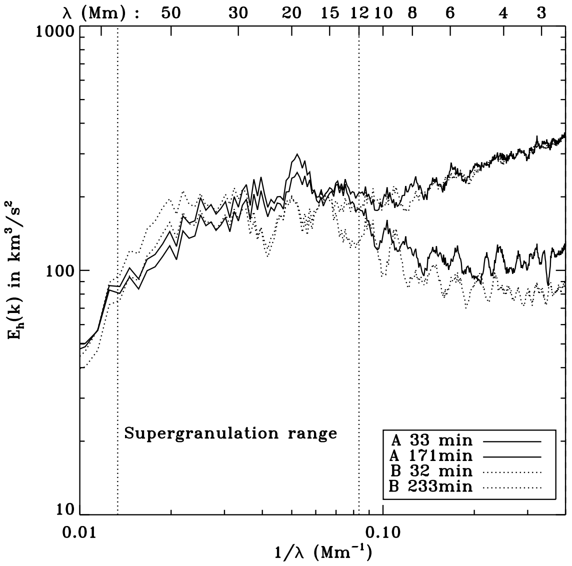

Fig. 5. Kinetic energy spectra of the horizontal velocity field during the emergence of two pores in the field-of-view. The solid line corresponds to the first series, at the end of which one pore has emerged. The dotted one corresponds to the second series, during which the second pore emerges. For each series, two time windows were used. The vertical dotted lines mark the 12.5–75 Mm range where the supergranulation peak is found (cf. Fig. 3). Here $N_x = 81$, $N_y = 82$ and $N_p = 1024$.

3. Velocity fields

3.1. Horizontal velocity fields

We give in Fig. 1 a typical view of the velocity field using a time average of 45 min, on which the supergranulation pattern is clearly visible. As is customary with any turbulent flow, it is crucial to investigate the spectral signature of these flows. The high quality of the data enables us to use the highest spatial and temporal resolutions available to granule tracking. Using the CST algorithm, as in Rieutord et al. (2008), we computed the kinetic energy spectrum $E_h(k)$ for various time windows for the horizontal motions as shown in Fig. 2. We recall its definition

$$\frac{1}{2}\left\langle \overline{v}_h^2 \right\rangle = \int_0^\infty E_h(k) dk \, ,$$

where $\overline{v}_h$ denotes the horizontal velocity field averaged over the time window during which the granule tracking is performed; $\langle\rangle$ should be an ensemble average; here it is a spatial average, assuming that the turbulent flow is ergodic.

For comparisons with other data sets, we plotted the dimensional values (in km^3/s^2) of the kinetic energy spectral densities in all the figures. Since this value depends on the normalisation of the Fourier transform, we give the details of the expressions used in the paper in Appendix A. In order to give a better spectral resolution, all spectra were computed using zero-padding. Thus, we give the size of the data (N_x, N_y) and the size of the padding area N_p for each spectrum.

These spectra are interesting for various reasons. First, we notice in Fig. 2 the prominent supergranulation peak centred at 30 Mm. This length scale is slightly shorter than the one measured by Rieutord et al. (2008), who found the maximum at 36.4 Mm. This change in the peak wavelength does not seem to be an artefact of the smaller field. Indeed, reducing the field on the data of Rieutord et al. (2008) to a size comparable to that of the present data, one still obtains a value of 36.4 Mm. The difference seems to result from an intrinsic variability. To verify this point, we analysed other data from various sources (other Hinode fields, some data from the TRACE satellite). The results, together with those obtained from SOHO/MDI data by Hathaway et al. (2000)[2] are summarised in Table 1. These data indeed show some variability both in the location of the peak and its amplitude. The fact that the small fields-of-view tend to give smaller values of the supergranulation scale may not be statistically significant.

Figure 2 also displays a plot of the individual spectra together with their average. These spectra provide further evidence of the strong variability of the horizontal velocity field even at the supergranulation scale. They are constructed from three-hours-averaged velocity fields. We note that they do not show any energy excess within the mesogranulation range, i.e. between 3 and 10 Mm. The absence of any specific spectral feature in this range is confirmed when other time windows are used (Fig. 3).

In Fig. 3 (left) we plot the mean spectra obtained with time windows ranging from 0.5 to 24 hours. Each spectrum is an average of all the independent spectra that could be extracted from the whole series. For instance the 0.5h time window allowed us to extract 66 independent spectra from the 33 hrs of data. Note that all spectra show a distinct rise at scales below 2.3 Mm ($1/\lambda > 0.43$ Mm^{-1}). This rise follows a linear law ($E_h(k) \sim k$) as expected from a two-dimensional uncorrelated noise. Hence we clearly find the spatial resolution limit imposed by granule tracking. This confirms the analysis performed on the numerical simulations by Rieutord et al. (2001), which suggested that granule tracking could not be used at scales smaller than 2.5 Mm.

The 30-minutes spectrum is the closest to an instantaneous one. This spectrum displays three features: (i) the supergranulation peak, (ii) a minimum in the kinetic energy density at 10 Mm and (iii) a slow monotonic increase towards the small scales. Feature (ii) was also found by Hathaway et al. (2000) in the Doppler measurements from SOHO/MDI; their spherical harmonic spectrum shows a minimum near $\ell = 400$ which corresponds to $\lambda = 11$ Mm, quite close to our value.

We note that the spectra obtained with time windows ranging from 30 min to 24 h almost superpose at large scales. However, shifting the attention to smaller scales, one finds the existence of a scale λ_t where the spectrum disconnects from the 30 min one (marked with black dots in Fig. 3). The time average acts as a low-pass filter which removes (or simply weakens) the flows on shorter time scales. The size of the time window can hence be used as a proxy of the correlation time of the flow at the scale marked by the dot. Figure 3 (right) shows the scale λ_t as a function of the time average associated with the time window. We find that the relationship between this length scale and the window size is close to a power law $\lambda_t \sim t^{2/5}$. As the correlation time is $\sim \lambda/v_\lambda$, we can relate v_λ and λ and find $v_\lambda \sim \lambda^{-3/2}$. This translates into a power law spectrum $E(k) \sim k^2$ for the kinetic energy. This exponent is typical of the range 7–25 Mm.

Finally, while processing other data sets to better evaluate the variability of the supergranulation peak, we came across the data recorded in the G-band by Hinode/SOT on 8 March 2007. Two series of images taken at [2:55, 5:45] UT and [6:00, 9:52] UT drew our attention. As shown in Fig. 5, the supergranulation peak has disappeared if we consider the shortest time sampling. In this figure we distinguished the two series because one pore is emerging at the end of the first series (around 4:40 UT) and the second pore emerges in the second series (around 6:18 UT). We note that the kinetic energy density in the supergranulation range has weakened at scales shorter than 33 Mm in the second series when the pair of pores has reached its steady state. We also observe that the TRACE data taken in April 2000 during the solar maximum also show a weaker supergranulation peak compared to the analogous data of 2007 taken at the solar minimum. Hence we note a trend that magnetic fields seem to markedly affect the amplitude of the supergranulation flows. This is likely connected with the anti-correlation between the size of the supergranules and the strength of the magnetic field observed by Meunier et al. (2007, 2008).

3.2. Vertical velocity fields

Let us now focus on the vertical velocity fields $v_z(x, y)$. As mentioned above, these are obtained from the Doppler effect and thus each pixel of the image gives a measure of this component of the velocity field. We now compute the horizontal spectral density of the vertical velocity, namely

$$\frac{1}{2}\left\langle \overline{v}_z^2 \right\rangle = \int_0^\infty E_v(k)dk$$

for various time averages.

Figure 6 shows the spectra of the Doppler radial velocity obtained with the bisector method after reconstruction of the line profile at 557.6 nm. We extracted velocities at two different altitudes. A line chord of 16 pm was used to sample a layer around an altitude of 80 km (Altrock et al. 1975; Berrilli et al. 2002) and a second chord of 8 pm, deeper in the line, was used to sample the atmosphere around 190 km. In order to detect potential spurious effects associated with the artificial flat-fielding operation, an additional set of spectra was computed from images not flat-fielded (Fig. 7).

First these spectra seem to follow $E_v(k) \sim k^2$ in the 2.5–7 Mm range. If the flat-fielding operation is correct, this power law may extend up to 30 Mm. Note that this slope is reminiscent of the power law found from the relationship between correlation time and the scale of horizontal velocities (see the previous section and Fig. 3-right). In terms of velocity, the k^2 power law for the spectral density implies $v_z \sim \sqrt{kE_v(k)} \sim k^{3/2} \sim \lambda^{-3/2}$.

As noted above, the quality of the data allowed us to investigate the subgranulation dynamics accurately for the first time. The absence of Earth atmospheric turbulence and the deconvolution of the images by the instrumental transfer function leads to high quality horizontal spectra of the vertical velocity. As shown by Fig. 6, we observe in this range of scales a decrease of the spectral density closely following a $k^{-10/3}$ power law. When the signal is slightly averaged over a 4-min interval, the cut-off is steeper and the exponent close to -4.

Concerning the granulation peak, the spectra show that the privileged scale is 1.7 Mm. The spectral kinetic energy density is around 100 km^3/s^2 at a mean altitude of ~80 km. At an altitude around 190 km, the same spectra show an amplitude of 50 km^3/s^2. This reduction of the spectral kinetic energy density is likely associated with the braking of upward motions which hit the stably stratified atmosphere.

To confirm these results with independent data, we used the third set presented in Sect. 2.2 taken with NFI around the FeI

---

[2] The amplitude of the peak for these data, given in between parenthesis, is an estimate resulting from a crude conversion of Doppler signal to horizontal velocities.

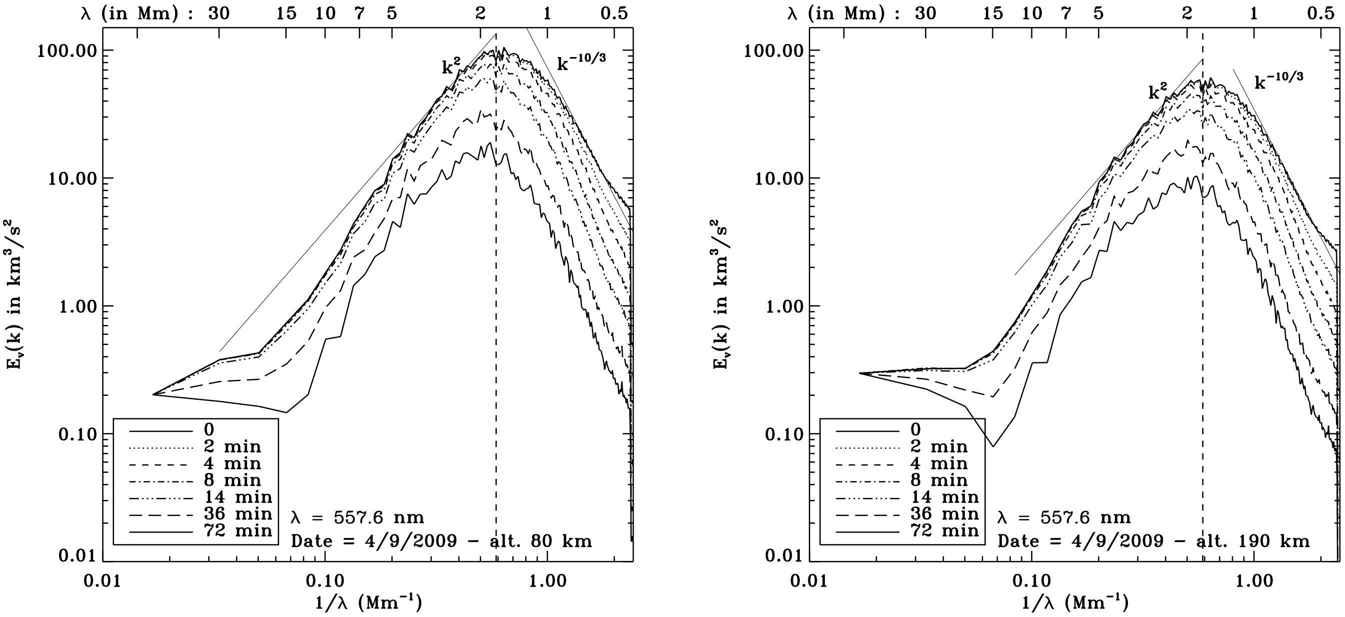

Fig. 6. Kinetic energy spectra of the vertical velocity field for various time windows. The vertical dotted line marks the maximum of the spectrum at $\lambda = 1.7$ Mm. Left: spectra computed with Doppler shifts taken with a line chord of 16 pm, corresponding to an mean altitude of 80 km. Right: same as left but for a chord of 8 pm, corresponding to an mean altitude of 190 km. The original images were flat-fielded according to the procedure described in Sect. 2.2. Here $N_x = N_y = N_p = 1024$.

line at 525.0 nm. Unlike the previous data at 557.6 nm we only had access to two wavelengths around the FeI line and had to derive the Doppler shift by the poor man's method, following Eq. 1. The results, shown in Fig. 8, are still interesting. With this method a k^2 power law is also obtained at large scales both on the 557.6 nm and 525.0 nm data. The latter data, which benefit from a good flat-field image, also indicate that the k^2 power law extends up to 30 Mm.

However, we find that the cut-off is sharper on the subgranulation side, not far from a $k^{-17/3}$ power law. This is presumably a residual of the small-scale cut-off of the intensity power spectrum, which follows the same power law (see below). This result suggests that the poor man's method is probably not appropriate for the computation of the small-scale radial velocity field.

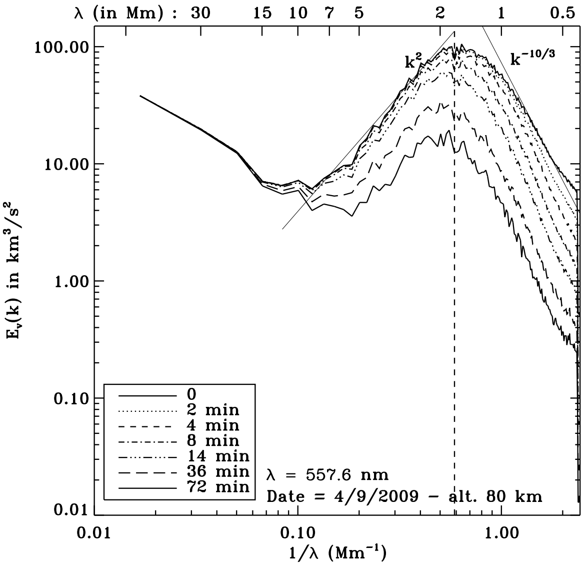

Fig. 7. Same as in Fig. 6- left, but with data not flat-fielded.

4. Intensity spectra

With the data sets presented in Sect. 2.1 and 2.2 we finally investigated the power spectrum of the horizontal intensity fluctuations defined according to

$$\frac{1}{2}\left\langle\overline{\delta I}^2\right\rangle = \int_0^\infty E_I(k)dk \,.$$

The spectra obtained from the blue continuum images at $\lambda = 450.4$ nm are shown in Fig. 9. The variations in the mesoscale range are characterised by a spectrum close to a k^2 power law, remarkably similar to the spectrum of vertical velocities. Assuming that the surface radiates like a blackbody, these fluctuations reveal those of temperature.

At scales smaller than a maximum located around the scale of 1.5 Mm, the power spectrum decreases steeply. In the subgranulation range, the spectral density almost follows a power law in k^{-3}. We note that these results agree with those of Wedemeyer-Böhm & Rouppe van der Voort (2009) as derived from their Fig. 9. Our longer time series provides a better statistic, which probably improves the determination of the large-scale side of the spectra.

We then used the images taken at 525.0316 nm with the NFI, whose width is 9 pm. It turned out that this light comes from the continuum just besides the FeI line at 525.0208 nm (Uitenbroek 2009). As shown in Fig. 9 (right), the intensity spectra show a steeper cut-off in the subgranulation range than for the previous data, close to a $k^{-17/3}$ law. We note that the granulation scale peak is at 2 Mm for this wavelength.

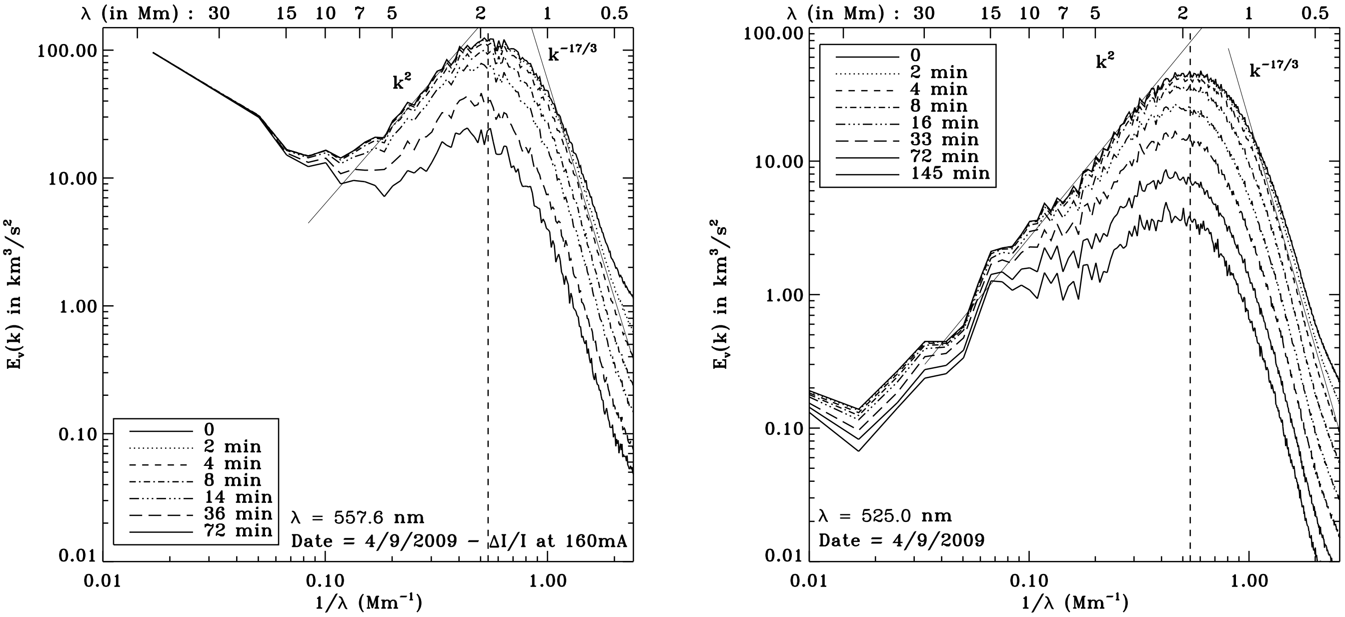

Fig. 8. Left: same as in Fig. 7, but with Doppler velocities computed with just two wavelengths in the line. Right: same as left but for $\lambda = 525.0$ nm (images are corrected using a flat-field image provided by the Hinode mission, $N_x = N_y = 704$ and $N_p = 1024$).

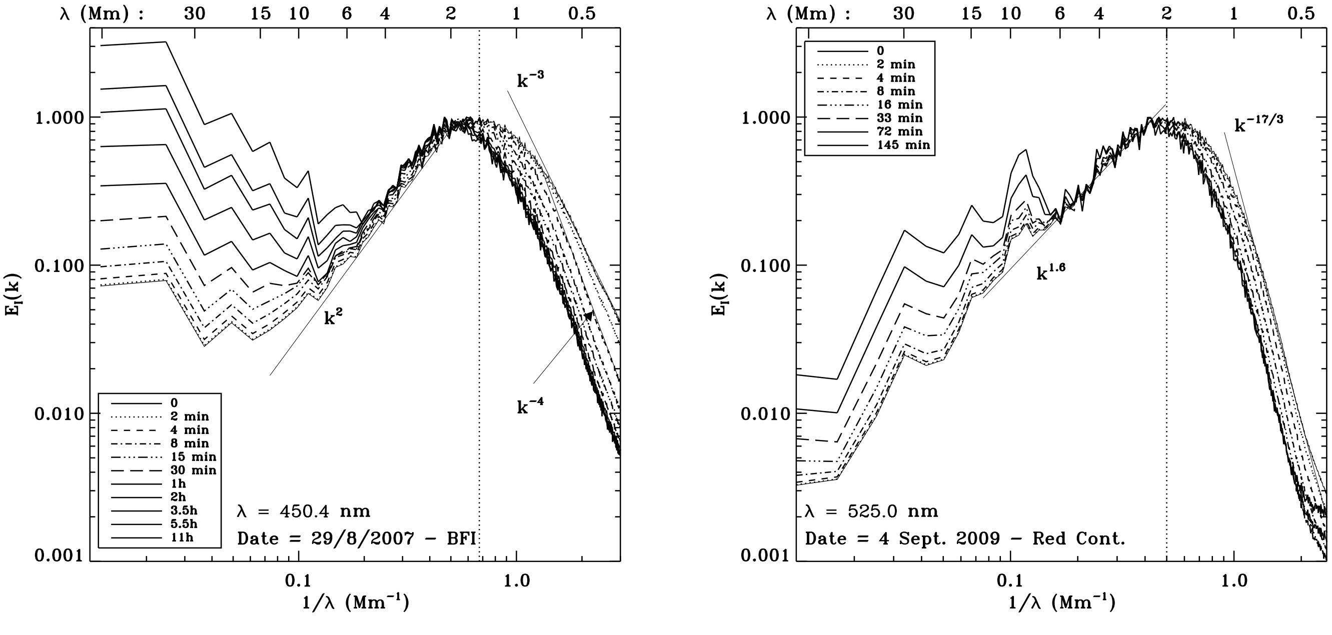

Fig. 9. Spectral energy density of the intensity field. Left: data from the BFI at 450.4 nm (spectral width of 0.22 nm sampling the blue continuum) for various time windows (data set of 29-31/8/2007). The spectra are normalised so that the amplitude of the granulation peak is unity. The vertical dotted line marks the position of the granulation peak determined with instantaneous spectra. Here $N_x = 941$, $N_y = 934$ and $N_p = 1024$. Right: data from the NFI at 525.0208+0.0108 nm (spectral width of 9 pm sampling the continuum on the red side of the line); here $N_x = N_y = 704$ and $N_p = 1024$.

Finally, the images taken at the blue side of the 525.0 nm FeI line are in fact very close to the line core, namely at 525.019 nm. Atmospheric models of Uitenbroek (2009) suggest that this intensity emerges at an altitude of 200 km above the continuum. The spectra shown in Fig. 10 show a clear shift of the granulation peak towards larger scales, namely 2.5 Mm. No power law arises in the meso-scales, while the subgranulation range shows a roundish cut-off with no clear power law.

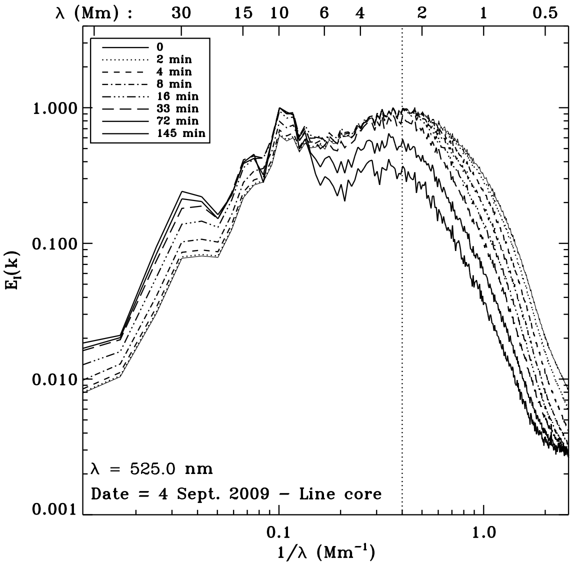

Fig. 10. Same as Fig. 9 -right, but with the NFI almost centred on the line core at $\lambda = 521.019$ nm.

5. Discussion and physical interpretation

5.1. Large scales

The foregoing results first confirm that the power spectra of horizontal flows at the Sun's surface are dominated by two scales corresponding to granulation at $\sim$1.7 Mm and supergranulation at $\sim$30 Mm. This result confirms the one of Hathaway et al. (2000), who used only one velocity component (the radial velocity) of the flow field. As far as the vertical velocity is concerned, the granulation scale clearly emerges at 1.7 Mm. On the large-scale side of granulation, we found that the vertical velocity field decreases like $\lambda^{-3/2}$ with the horizontal length scale λ, corresponding to a k^2-law for the associated kinetic energy spectral density. This law seems to be valid up to the supergranulation scale since its prediction of a supergranule vertical velocity corresponds to the value of 30 m s^{-1} found by Hathaway et al. (2002) with MDI/SOHO data. Note that this conclusion holds only if the flat-field operations on the images did not damage the data.

The k^2-scaling law of vertical kinetic energy can be related to the scaling law of the horizontal kinetic energy spectral density using physical arguments. Indeed, mass conservation (see below Eq. 2) implies that $v_z/H \sim v_h/\lambda$, where H is the vertical scale height. If H is independent of λ, and since $v_z \sim \lambda^{-3/2}$, then $v_h \sim \lambda^{-1/2}$, meaning that $E_h(k) \sim$ const. This law is approximately consistent with the horizontal flow data: as shown by the 30-minutes spectrum in Fig. 3, the spectral density $E_h(k)$ does not vary very much in the 2.5–20 Mm range, where it stays between 190 and 260 km^3/s^2.

To conclude on the k^2 power law, we note that it also appears in the intensity fluctuation spectrum obtained with the broadband filter in the blue continuum. This looks like a strong correlation between buoyancy fluctuations traced by intensity fluctuations and vertical velocities. However, we observe that this scaling is not as conspicuous at another wavelength with a narrower filter, which likely samples different layers (see discussion below).

The derived horizontal flows may also be used to obtain some information on the scale height of the variations of the vertical velocity at the scale of supergranulation. Assuming that the anelastic approximation can be used at these scales (it means that acoustic waves are filtered out), we can write the mass conservation as

$$\partial_z v_z = -v_z \partial_z \ln\rho - \boldsymbol{\nabla}_h \cdot \boldsymbol{v}_h\,, \qquad (2)$$

where $\boldsymbol{v}_h$ is the horizontal velocity field and ρ is the background density. Using the simple model of Simon et al. (1991) for a horizontal divergent source, namely $v_r = vr/R\exp(-r^2/R^2)$, we could estimate for a well-formed supergranule that the divergence is approximately 10^{-4} s^{-1}. From Stein & Nordlund (1998), $\partial_z \ln\rho \sim 2.4$ Mm^{-1} near the surface. Then, using the estimate of 30 m s^{-1} for the vertical velocity at this scale, we find that the vertical scale height is $\sim$ 1 Mm, which indicates that the supergranulation flow is likely shallow. This qualitative estimate agrees with recent local helioseismic inferences based on Hinode data (Sekii et al. 2007), which indicate that the imprint of supergranulation flows disappears around 3 Mm below the surface. Note that the foregoing exercise has been done using typical values of all quantities and just gives a first impression. To go further and get a more reliable view, this calculation should be applied to a large sample of supergranules.

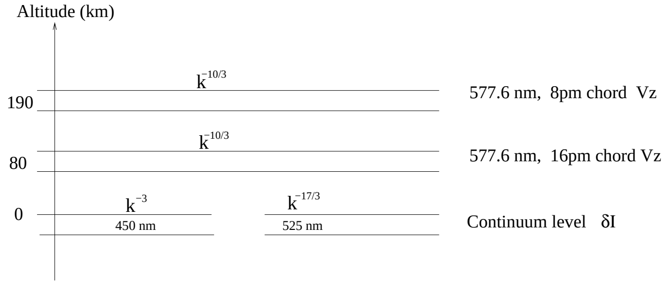

Fig. 11. Schematic view of the results. We indicate the layers where power laws are perceptible in the subgranulation range.

5.2. Sub-granulation scales: an injection-diffusive range ?

On the other side of the granulation peak, in the subgranulation range, the power spectrum of vertical velocity closely follows a $k^{-10/3}$ law, which steepens to k^{-4} with time averaging, while the intensity variance spectrum seems to follow either a k^{-3} law or a $k^{-17/3}$ law depending on the data set used. These results are summarised in Fig. 11.

A natural question to ask is what these scaling laws tell us about the physics of the solar surface. It is indeed well established that a variety of characteristic power law regimes can be derived for all kinds of turbulent complex flows depending on the detailed physical processes at work in the flow (e.g. shear turbulence (Lumley 1967; Lohse & Müller-Groeling 1996), stably and unstably stratified turbulence (Obukhov 1959; Bolgiano 1959, 1962; L'vov 1991), MHD turbulence (Schekochihin et al. 2008, and references therein)) and on the relevant range of scales (e.g. injection, inertial or dissipation range) for each physical field in the problem. In the paragraphs below, we therefore attempt to determine if the observed subgranulation scaling exponents betray a particular flow regime.

First of all, considering the many differences between homogeneous, isotropic, incompressible turbulence and solar surface turbulence at observable scales (Nordlund et al. 1997; Petrovay 2001; Rincon 2007), there is no real reason to expect that the Kolmogorov phenomenology of turbulence (which predicts a

$k^{-5/3}$ power law for the velocity field in the inertial range) applies in the vicinity of the granulation scale.

A possible interpretation for the joint observation of the $-10/3$ and $-17/3$ exponents is in terms of buoyant dynamics in the injection range of solar surface turbulence (i.e. not in the inertial range). Let us assume that (i) buoyancy fluctuations are directly proportional to temperature fluctuations (i.e. pressure fluctuations are not influential) and that (ii) the dynamic is dominated by a balance between inertial terms (or acceleration) and buoyancy forcing in the momentum equation. Further assuming that velocity and temperature perturbations have the following horizontal scale λ dependence

$$v_h(\lambda) \sim \lambda^\alpha, \qquad v_z(\lambda) \sim \lambda^\beta, \qquad \delta T(\lambda) \sim \lambda^\gamma$$

and that vertical variations are controlled by the typical pressure or density scale height H independent of λ, mass conservation imposes that $v_z/H \sim v_h/\lambda$, implying $\alpha = \beta + 1$. Assuming finally the locality of non-linear interactions, (i) and (ii) translate into the dynamical balance

$$v_h v_z/\lambda + v_z^2/H \sim \delta T \ ,$$

hence $\gamma = 2\beta$. Now, if the horizontal fluctuations of temperature follow a $k^{-17/3}$ spectrum, i.e. $\delta T \sim \sqrt{\lambda^{17/3-1}} \sim \lambda^{7/3}$, then $\gamma = 7/3, \beta = 7/6$ and the horizontal spectrum of the vertical velocity is $E_v(k) \sim k^{-10/3}$, just as observed[3]. Hence it is possible to relate the horizontal fluctuations of intensity at the continuum level to those of the vertical velocity in the upper layers (80 km or 190 km above) in the subgranulation range.

Still, this is only one half of the story, since the argument does not predict the $-17/3$ slope for the intensity spectrum (it uses it as an input). This is because two dominant balances are required to determine scaling laws consistently in active scalar turbulence. In the context of thermal convection, the second balance is obtained by isolating the dominant physical effects in the temperature equation or, to be more precise, in the Yaglom equation (Rincon 2006), which is the analog of the von Kármán-Howarth equation for the statistics of scalars. In the Boussinesq approximation (which is not suitable for the problem of solar convection), a $k^{-17/3}$ spectrum for temperature fluctuations can only be obtained if (i) the following low Péclet number dominant balance[4]

$$v_z \,\partial_z \langle T\rangle \sim \kappa\, \Delta \delta T \qquad (3)$$

is assumed in the temperature equation (where κ is the thermal diffusivity), i.e. temperature fluctuations are the diffusive response to velocity fluctuations advecting a mean, slowly varying temperature profile $\langle T\rangle$ and (ii) the velocity fluctuations are not influenced by temperature fluctuations and have a $k^{-5/3}$ spectrum (Kolmogorov inertial range), i.e. $v_z \sim \lambda^{1/3}$. Then, $\delta T \sim \lambda^2 v_z \sim \lambda^{7/3}$, or equivalently $E_I(k) \sim k^{-17/3}$. This is the so-called inertial-diffusive regime (see e.g. Lesieur 1990). Note that for any velocity spectrum slope steeper than -5/3 (say -10/3) Eq. (3) predicts a spectrum much steeper than $k^{-17/3}$ for temperature fluctuations. Hence, it remains to be understood at this stage how the two slopes observed at the solar surface can be made fully consistent using dynamical arguments.

Another interesting result regarding the sub-granulation range dynamics is that the intensity fluctuations taken with the BFI in the "blue continuum" at 450 nm have a much weaker spectral cut-off close to a k^{-3} power law (k^{-4} if slightly averaged) than those taken in the continuum near the FeI line at 525 nm. This is quite surprising, because the fluid layer contributing most to the blue continuum should be quite similar to the one contributing to the 525 nm continuum from which the $k^{-17/3}$ spectrum was derived. Beside the simple wavelength difference, which indicates a slighly lower contributing layer for the 450 nm radiation, the most obvious difference between the two signals comes from the spectral width of the filters. The width of the NFI of 9 pm is such that the continuum near 525 nm is "pure", while the width of the BFI at 450.45 nm is 220 pm and includes a few absorption lines. For this reason, the layers contributing to the light collected in the two wavebands could be somewhat different. At the moment we have no obvious explanation of these two different cut-offs for the intensity spectrum in the continuum. Of course we cannot totally exclude some unexpected bias in the data processing, but if the result is confirmed by independent approaches, detailed numerical simulations of the dynamics are likely the only way to elucidate this puzzle.

For the sake of completeness, we mention that a k^{-3} spectrum could be a simple signature of a physically smooth temperature field, which can be expanded in Taylor series. Indeed, if $T(\lambda) = T(0) + \lambda \nabla_h T_{|\lambda=0}$ then $\delta T = T(\lambda) - T(0) \sim \lambda$, or equivalently $E_I(k) \sim k^{-3}$. But, similarly to the argument presented previously, we underline that this scaling is not fully consistent with a $k^{-10/3}$ scaling for the velocity field if a dominant balance between inertia and buoyancy is assumed in the momentum equation.

The previous theoretical arguments should of course not be taken at face value. They simply suggest that it might be possible to construct some sort of "injection-diffusive" turbulent regime characteristic of the sub-granulation range, and serve to illustrate that the standard framework of incompressible homogeneous isotropic turbulence is probably too restrictive to theoretically explain the observations of the thermal boundary layer at the solar surface.

These new observational measurements for the subgranulation range definitely call for a deeper investigation. A detailed theoretical understanding of the solar power spectrum at the beginning of the subgranulation range 0.1–1 Mm might be obtained by re-analysing existing numerical simulations of solar granulation (Stein & Nordlund 1998), looking for the dominant terms in the temperature (or energy) equation[5]. Another possibility would be to perform idealised high-resolution numerical simulations of thermal turbulence done in the low-Péclet approximation (Thual 1992; Lignières 1999) to better understand this complex and fairly unusual turbulence regime from the theoretical point of view.

6. Conclusions

The power spectrum of surface flows at the Sun's surface has been investigated using mainly image series from the Hinode/SOT instrument. The results may be summarised as follows.

---

[3] Assuming isotropy, the dynamical balance would instead read $v_z^2/\lambda \sim \delta T$, leading to $E_v(k) \sim k^{-13/3}$ for $E_I(k) \sim k^{-17/3}$.This argument can be formalised using a generalised exact von Kármán-Howarth-Kolmogorov equation for thermal convection (Rincon 2006).

[4] The Péclet number of a thermal eddy is the ratio between its thermal diffusion time and its typical turnover time. It is effectively of the order of one or smaller in the sub-granulation range.

[5] It is remarkable that some of the early numerical simulations by Nordlund et al. (1997) seemed to produce a $k^{-17/3}$ scaling for intensity fluctuations.

1. The smallest scales, i.e. the subgranulation range, can be investigated for the first time without a seeing effect and using corrections of the MTF of the instrument. On the one hand, the spectral cut-off of intensity fluctuations is similar to a $k^{-17/3}$ power law for images taken with a narrow filter (width $\sim$ 9 pm) in the continuum on the red side of the 525 nm FeI line and to k^{-3} for images taken with the broadband filter (width $\sim$ 220 pm) around 450.45 nm. On the other hand, the vertical velocity horizontal spectrum measured 80 km or 190 km above the continuum at 557.6 nm shows a steep cut-off in $k^{-10/3}$, which can be related to the $k^{-17/3}$ power law by invoking a balance between buoyancy and inertia. The values of the two scaling exponents suggest that the temperature fluctuations impact the dynamics at a scale well below the one determined by the unit Péclet number. Finally, we also note the decrease of the granulation peak amplitude with altitude, possibly betraying the deceleration of the upflows.
2. The granulation spectral peak at 1.7 Mm is conspicuous in the vertical velocity spectrum. The location of the intensity spectrum peak depends on the wavelength: it is close to 1.5 Mm in the blue continuum at 450 nm, 2 Mm in the continuum near 525 nm, and to 2.5 Mm in the core of the FeI line at 525.0 nm, which probes the dynamics in a layer 200 km above the continuum.
3. Moving to the large scales, we note that the spectral density of vertical kinetic energy decreases as k^2 with decreasing k (equivalently, the amplitude of v_z decreases as $\lambda^{-3/2}$ with the horizontal scale λ). This k^2 power law also emerges from the relationship between the scale and the correlation time of the horizontal flows. Furthermore we note that the spectral density of intensity fluctuations in the blue continuum also scales like k^2 in the 2.5–10 Mm range.
4. The power spectrum of horizontal flows has been explored in the 2.5–40 Mm range. It clearly reveals the supergranulation peak as well as the large-scale side of the granulation peak. These observations confirm in passing the result of the numerical simulations of Rieutord et al. (2001) that granule tracking cannot determine plasma flows at scales below ~2.5 Mm. The energy density minimum is found at a scale of 12 Mm. These results confirm with a completely different technique the spherical harmonics spectra obtained by Hathaway et al. (2000) from dopplergrams. Focusing on the supergranulation peak, we could estimate its amplitude to be in the range of 200–700 km^3/s^2 and show its strong variability. From Figs. 3 and 5 we may add that the visible part of the granulation peak points to an amplitude in the range of 200–400 km^3/s^2. Interestingly enough, we discovered that the emergence of a pair of pores is able to erase the supergranulation peak completely, which points out the sensitivity of the supergranulation amplitude flow to the ambient magnetic field. Finally, combining all the data, we tentatively estimated the scale-height of the vertical velocity field at the supergranulation horizontal scale. We found a scale height of approximately 1 Mm, indicating that supergranules are likely surface flows. However, this estimate should be verified for a number of supergranules to obtain a statistically robust value.

These observational results provide a set of landmarks that should be recovered by future numerical simulations. Future observational work will focus on the large-scale side of the supergranulation peak to determine what scaling law, if any, controls the very large-scale dynamics of the Sun between supergranulation and differential rotation. Another point deserving a detailed investigation is the dynamical influence of the magnetic fields on the surface flows and their power spectrum.

Acknowledgements. We are grateful to the Hinode team for the possibility to use their data. Hinode is a Japanese mission developed and launched by ISAS/JAXA, collaborating with NAOJ as a domestic partner, NASA and STFC (UK) as international partners. Scientific operation of the Hinode mission is conducted by the Hinode science team organised at ISAS/JAXA. This team mainly consists of scientists from institutes in the partner countries. Support for the post-launch operation is provided by JAXA and NAOJ (Japan), STFC (U.K.), NASA, ESA, and NSC (Norway).This work was (partly) carried out at the NAOJ Hinode Science Center, which is supported by the Grant-in-Aid for Creative Scientific Research "The Basic Study of Space Weather Prediction" from MEXT, Japan (Head Investigator: K. Shibata), generous donations from Sun Microsystems, and NAOJ internal funding.

We thank François Lignières for several interesting comments and remarks on the manuscript. We are also very grateful to Han Uitenbroek who provided us with simulations results of line formation in the Sun's atmosphere. This work was supported by the Centre National de la Recherche Scientifique (C.N.R.S., UMR 5572), through the Programme National Soleil Terre (P.N.S.T.).

References

Altrock, R. C., November, L. J., Simon, G. W., Milkey, R. W., & Worden, S. P. 1975, Solar Phys., 43, 33
Berrilli, F., Consolini, G., Pietropaolo, E., et al. 2002, A&A, 381, 253
Bolgiano, R. 1959, J. Geophys. Res., 64, 2226
Bolgiano, R. 1962, J. Geophys. Res., 67, 3015
Crouch, A. D., Charbonneau, P., & Thibault, K. 2007, ApJ, 662, 715
Danilovic, S., Gandorfer, A., Lagg, A., et al. 2008, A&A, 484, L17
Gizon, L. & Birch, A. C. 2005, Living Reviews in Solar Physics, 2, 6
Green, C. A. & Kosovichev, A. G. 2006, ApJ, 641, L77
Green, C. A. & Kosovichev, A. G. 2007, ApJ, 665, L75
Hathaway, D., Beck, J., Bogart, R., et al. 2000, Solar Phys., 193, 299
Hathaway, D. H., Beck, J. G., Han, S., & Raymond, J. 2002, Solar Phys., 205, 25
Ichimoto, K., Tsuneta, S., Suematsu, Y., et al. 2004, in Society of Photo-Optical Instrumentation Engineers (SPIE) Conference, Vol. 5487, Optical, Infrared, and Millimeter Space Telescopes, ed. J. C. Mather, 1142–1151
Lesieur, M. 1990, Turbulence in fluids (Kluwer)
Lignières, F. 1999, A&A, 348, 933
Lohse, D. & Müller-Groeling, A. 1996, Phys. Rev. D, 54, 395
Lumley, J. L. 1967, Phys. Fluids, 10, 855
L'vov, V. S. 1991, Phys. Rev. Lett., 67, 687
Meunier, N., Roudier, T., & Rieutord, M. 2008, A&A, 488, 1109
Meunier, N., Roudier, T., & Tkaczuk, R. 2007, A&A, 466, 1123
Nordlund, A., Spruit, H., Ludwig, H.-C., & Trampedach, R. 1997, A&A, 328, 229
Nordlund, Å., Stein, R. F., & Asplund, M. 2009, Living Reviews in Solar Physics, 6, 1
November, L. J., Toomre, J., Gebbie, K., & Simon, G. W. 1981, ApJ, 245, L123
Obukhov, A. 1959, Dokl. Akad. Nauk. SSR, 125
Petrovay, K. 2001, Space Science Reviews, 95, 9
Rast, M. P. 2003, ApJ, 597, 1200
Rieutord, M., Ludwig, H.-G., Roudier, T., Nordlund, A., & Stein, R. 2002, Nuovo Cimento C Geophysics Space Physics C, 25, 523
Rieutord, M., Meunier, N., Roudier, T., et al. 2008, A&A, 479, L17
Rieutord, M., Roudier, T., Ludwig, H.-G., Nordlund, Å., & Stein, R. 2001, A&A, 377, L14
Rieutord, M., Roudier, T., Malherbe, J. M., & Rincon, F. 2000, A&A, 357, 1063
Rieutord, M., Roudier, T., Roques, S., & Ducottet, C. 2007, A&A, 471, 687
Rieutord, M. & Zahn, J.-P. 1997, ApJ, 474, 760
Rincon, F. 2006, Journal of Fluid Mechanics, to appear, 1
Rincon, F. 2007, in IAU Symposium, Vol. 239, IAU Symposium, ed. F. Kupka, I. W. Roxburgh, & K. L. Chan, 58
Rincon, F., Lignières, F., & Rieutord, M. 2005, A&A, 430, L57
Rincon, F. & Rieutord, M. 2003, in SF2A-2003: Semaine de l'Astrophysique Francaise, ed. F. Combes, D. Barret, T. Contini, & L. Pagani, 103
Schekochihin, A. A., Cowley, S. C., & Yousef, T. A. 2008, in IUTAM Bookseries, Vol. 4, IUTAM Symposium on Computational Physics and New Perspectives in Turbulence, ed. Y. Kaneda (Springer Netherlands), 347–354
Sekii, T., Kosovichev, A. G., Zhao, J., et al. 2007, Pub. Astron. Soc. Jap., 59, 637
Shine, R., Simon, G., & Hurlburt, N. 2000, Solar Phys., 193, 313
Simon, G. & Leighton, R. 1964, ApJ, 140, 1120
Simon, G., Title, A., & Weiss, N. 1991, ApJ, 375, 775
Stein, R. & Nordlund, A. 2000, Solar Phys., 192, 91

Stein, R. F., Georgobiani, D., Schafenberger, W., Nordlund, Å., & Benson, D. 2009, in American Institute of Physics Conference Series, ed. E. Stempels, Vol. 1094, 764–767
Stein, R. F. & Nordlund, Å. 1998, ApJ, 499, 914
Straus, T. & Bonaccini, D. 1997, A&A, 324, 704
Straus, T., Deubner, F.-L., & Fleck, B. 1992, A&A, 256, 652
Suematsu, Y., Tsuneta, S., Ichimoto, K., et al. 2008, Solar Phys., 249, 197
Thual, O. 1992, J. Fluid Mech., 240, 229
Uitenbroek, H. 2009, Private Communication
van der Borght, R. 1974, Aus. J. Phys., 27, 481
Wedemeyer-Böhm, S. & Rouppe van der Voort, L. 2009, A&A, 503, 225

Appendix A: Absolute spectra

In this paper, we give the kinetic energy density spectra with their absolute values in km^3/s^2. To facilitate future comparisons, we document the way these spectral densities are computed in detail. We recall that the kinetic energy spectrum $E(k)$ is defined as

$$\frac{1}{2}\left\langle v^2\right\rangle = \int_0^\infty E(k)dk\,. \tag{A.1}$$

It is related to the Fourier transform of the velocity components by

$$\left\langle \hat{v}_i^*(\boldsymbol{k})\hat{v}_j(\boldsymbol{k}')\right\rangle = \phi_{ij}(\boldsymbol{k})\delta(\boldsymbol{k}-\boldsymbol{k}')\,, \tag{A.2}$$

where $\phi_{ij}(\boldsymbol{k})$ is the Fourier transform of the two-point correlation function of the velocities, namely, $Q_{ij}(\boldsymbol{r}) = \left\langle v_i(\boldsymbol{x})v_j(\boldsymbol{x}+\boldsymbol{r})\right\rangle$. δ is the Dirac distribution. In two dimensions (our case here), $E(k)$ and ϕ_{ij} are related by

$$E(k) = \frac{1}{2}k\int_0^{2\pi}\phi_{ii}(\boldsymbol{k})d\theta_k\,, \tag{A.3}$$

where θ_k is the polar angle of $\boldsymbol{k}$. The numerical 2D-Fourier transform (like in the IDL software) is defined as

$$\tilde{f} = \frac{1}{N_xN_y}\sum_{x,y} f(x,y)e^{-2i\pi(k_xx+k_yy)}\,, \tag{A.4}$$

which means that the Dirac distribution in a discrete way reads

$$\tilde{\delta} = \frac{1}{N_xN_y}\sum_{x,y} e^{-2i\pi(k_xx+k_yy)}\,, \tag{A.5}$$

Now, spectral quantities in turbulence theory usually use

$$\hat{f}(\boldsymbol{k}) = (2\pi)^{-2}\int f(\boldsymbol{r})e^{-i\boldsymbol{k}\cdot\boldsymbol{r}}dxdy \tag{A.6}$$

as the definition of the 2D-Fourier transform. Setting $\boldsymbol{k} = 2\pi\boldsymbol{k}'$ then

$$\hat{f}(\boldsymbol{k}) = (2\pi)^{-2}\int f(\boldsymbol{r})e^{-2i\pi\boldsymbol{k}'\cdot\boldsymbol{r}}dxdy\,, \tag{A.7}$$

The correspondence is accordingly

$$\hat{f}(\boldsymbol{k}) = \tilde{f}(\boldsymbol{k}')N_xN_yp^2/(2\pi)^2 \quad\text{and}\quad \delta(\boldsymbol{k}) = \tilde{\delta}N_xN_yp^2/(2\pi)^2\,, \tag{A.8}$$

where N_x and N_y are the size of the data. p is the linear size of the pixel. We wish to derive the correct normalisation of $E(k)$ which is that of $\phi_{ii}(\boldsymbol{k})$. We note that $\phi_{ii}(\boldsymbol{k})$ is the ratio of the squared norm of the Fourier components of the velocity divided by the Dirac distribution. Using the preceeding normalisation for both $\hat{v}$ and $\delta(\boldsymbol{k})$, we find that

$$\phi_{ii}(\boldsymbol{k}) = \frac{|\hat{v}|^2}{\delta(\boldsymbol{k})} = \frac{|\tilde{v}|^2(N_xN_y)^2p^4(2\pi)^2}{(N_xN_y)p^2(2\pi)^4} = |\tilde{v}|^2N_xN_yp^2/(2\pi)^2\,. \tag{A.9}$$

If we restrict our case to a square data set ($N_x = N_y = N$), then

$$E(k) = \frac{1}{2}\int\phi_{ii}(\boldsymbol{k})kd\theta_k = \frac{1}{2}\sum_{\forall k'\in[k,k+dk]/2\pi}|\tilde{v}(k')|^2\frac{2\pi}{Np}\frac{N^2p^2}{(2\pi)^2}\,,$$

where we noticed that the dimensional wavenumber k and the non-dimensional one are related by a factor $2\pi/Np$. Finally,

$$E(k) = \frac{1}{2}\frac{Np}{(2\pi)}\sum_{\forall k'\in[k,k+dk]/2\pi}|\tilde{v}_x(k')|^2 + |\tilde{v}_y(k')|^2\,, \tag{A.10}$$

where $\tilde{v}_x$ and $\tilde{v}_y$ are the discrete Fourier transform of v_x and v_y. Note that the summation $\sum_{\forall k'\in[k,k+dk]/2\pi}$ implies that the k' factor of the surface element $k'd\theta_kdk'$ is automatically taken into account. Sometimes the quantity $P(k) = \sqrt{kE(k)}$ is used; here

$$P(k) = \sqrt{\frac{1}{2}\sum_{\forall k'\in[k,k+dk]/2\pi}k'|\tilde{v}|^2}\,. \tag{A.11}$$

Effect of zero padding: the Fourier transforms are done on a square of size $N\times N$, while the data usually occupy a rectangle of the size of $N_x{\times}N_y$ ($N_x \leq N, N_y \leq N$); the energy of the Fourier modes is thus a fraction N_xN_y/N^2 of the total. Hence, to obtain spectra which are independent of the zero padding, we need to multiply the resulting spectral densities by $N^2/(N_xN_y)$ so that

$$E(k) = \frac{N^3p}{4\pi N_xN_y}\sum_{\forall k'\in[k,k+dk]/2\pi}|\tilde{v}|^2\,, \tag{A.12}$$

Effect of the normalisation of the Fourier Transform: if the Fourier Transform is multiplied by a factor A, then $E(k)$ is multiplied by A and $P(k)$ is multiplied by a factor $\sqrt{A}$. The $P(k)$ spectrum has no absolute significance.